

Skeleton-Based Mutually Assisted Interacted Object Localization and Human Action Recognition

Liang Xu, Cuiling Lan, *Member, IEEE*, Wenjun Zeng, *Fellow, IEEE*, and Cewu Lu, *Member, IEEE*

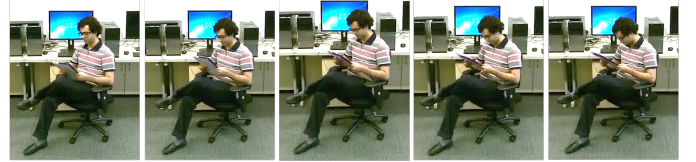
Abstract—Skeleton data carries valuable motion information and is widely explored in human action recognition. However, not only the motion information but also the interaction with the environment provides discriminative cues to recognize the action of persons. In this paper, we propose a joint learning framework for mutually assisted “interacted object localization” and “human action recognition” based on skeleton data. The two tasks are serialized together and collaborate to promote each other, where preliminary action type derived from skeleton alone helps improve interacted object localization, which in turn provides valuable cues for the final human action recognition. Besides, we explore the temporal consistency of interacted object as constraint to better localize the interacted object with the absence of ground-truth labels. Extensive experiments on the datasets of SYSU-3D, NTU60 RGB+D and Northwestern-UCLA show that our method achieves the best or competitive performance with the state-of-the-art methods for human action recognition. Visualization results show that our method can also provide reasonable interacted object localization results.

Index Terms—Skeleton-Based Action Recognition, Interacted Object Localization, Joint Learning.

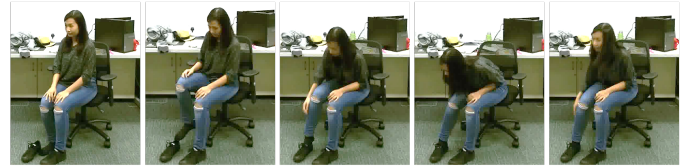
I. INTRODUCTION

Human action recognition is a pivotal problem in video-based tasks, such as human-computer interaction, intelligent surveillance, video understanding and robotics [1], [2], [3]. In particular, skeleton-based action recognition shows its superiority and develops rapidly in recent years [4], [5], [6], [7], [8], [9], [10], [11], [12]. Skeleton data contains the 2D or 3D coordinates of the human key joints, which is a high level, efficient, robust and privacy-friendly representation for human poses and motion information. Besides, the access of skeleton data becomes easier thanks to the development of depth cameras and human pose estimation algorithms.

Powered by deep learning especially graph convolutional network, skeleton data has been proved to be effective for human action recognition. However, skeleton input alone may encounter several problems. First, skeleton sequences could be deficient and ambiguous under certain circumstances. For example, given a standing-still person talking to another person or watching a television, their action categories differ greatly



(a) Non-discriminative skeleton sequence



(b) Ambiguous interacted object localization

Fig. 1. Two examples of action “read” and “wear a shoe”. For (a), the skeleton sequence alone is not discriminative enough for recognizing “read”. Integrating object information, *i.e.*, the book, can facilitate the recognition of “read”. For (b), the skeleton data could be ambiguous for localizing the interacted object without the knowledge of the action type (both the shoe and the chair could be interacted with).

yet the skeleton sequences have little difference. Second, these methods neglect the human-environment interactions, which play indispensable roles to model human actions [13], [14]. Human-object interactions account for the majority of daily human activities [15] and the object knowledge can serve as strong and complementary cues. Third, skeleton data cannot handle those fine-grained action recognition tasks, such as analyzing the behavior of customers picking up commodities in a store. Therefore, aggregating skeleton data with its interacted object is intuitively helpful in dealing with the aforementioned challenges.

Nonetheless, interacted object localization in videos is still an open and less explored problem. For *image-based* human object interaction detection, Gkioxari *et al.* [16] predict the interacted object location based on the appearance feature of a detected person with the supervision of volumes of labeled interacted person-object box pairs. However, in video action datasets, labeling the bounding boxes of interacted person-object pairs is quite expensive and frustrating. Luckily, skeleton sequence provides some cues for localizing where the interacted object is, such as the distance between the human skeleton and the objects, the active human parts for localizing a rough object area. Besides, temporal motion and consistency of interacted object could also be explored to benefit the localization.

In this paper, in order to jointly exploit the interacted object and skeleton data for robust human action recognition, we

This work was done while Liang Xu was an intern with Microsoft Research Asia.

Liang Xu and Cewu Lu are with the Department of Electrical and Computer Engineering, Shanghai Jiao Tong University, Shanghai, 200240, China. E-mail: liangxu@sjtu.edu.cn; lucewu@sjtu.edu.cn

Cuiling Lan and Wenjun Zeng are with Microsoft Research Asia. E-mail: culan@microsoft.com; wezeng@microsoft.com

Corresponding author: Cuiling Lan.

introduce an auxiliary task called “*skeleton-based interacted object localization*”, *i.e.*, localize the interacted object of a given person based on the skeleton data in an unsupervised manner. Skeleton based interacted object localization shares the same difficulties as human action recognition. As demonstrated in Fig. 1(b), the girl is sitting on a chair and wearing a shoe simultaneously. The skeleton data may be ambiguous and insufficient for localizing the interacted object, unless the action type is given. Moreover, action type carries valuable semantic information to indicate the interaction style and can help filter improbable objects, thus could boost the object localization performance.

We design a joint learning framework for “interacted object localization” and “human action recognition”. The two tasks are serialized together and collaborate to mutually assist each other. Fig. 2 illustrates our framework with skeleton sequences and object proposals as input. An object detector is first applied on each frame to obtain the *object proposals/candidates* (*i.e.*, positions and categories of objects) for the subsequent interacted object localization. A skeleton-only action recognition model generates a preliminary action classification score, followed by a joint learning procedure of (a) Action Type Assisted Interacted Object Localization and (b) Interacted Object Assisted Human Action Recognition.

We summarize our main contributions as follows.

- We design a joint learning framework for interacted object localization and human action recognition based on skeleton data without ground-truth of interacted object.
- We explore the preliminary action type cues and the consistency characteristic of interacted object across time to promote the reliable localization of interacted object, which in turn helps action recognition.

We evaluate the performance of our proposed method on three widely used datasets for skeleton-based action recognition: SYSU-3D [17], NTU60 RGB+D [18] and Northwestern-UCLA [19]. Extensive experiments show that: (1) integrating interacted object information can significantly boost the performance of human action recognition; (2) incorporating action type cues with skeleton data enhances the performance of interacted object localization, which in turn helps human action recognition; (3) reasonable interacted object localization results are obtained even without interacted object labels. We will release our code and models upon acceptance.

II. RELATED WORK

A. Video Action Understanding

Action recognition is fundamental in video-based tasks with many approaches proposed [20], [21], [22], [23], [24], [25], [26], [27], [28], [29] and datasets [30], [31], [18], [17], [19], [32], [33], [34]. We notice that there is also a trend for more fine-grained action understanding, from video classification [20], [21] to spatial-temporal action detection [32], [35], [36], [14], and human-part level action recognition [15]. However, so far, interacted object localization together with skeleton motion for robust human action recognition is less explored. We propose a joint learning framework of interacted object localization and action recognition and enable their mutual promotion.

B. Skeleton-based Action Recognition

Skeleton-based action recognition attracts much attention. Traditional approaches [37], [38], [18], [39], [40], [41] design hand-crafted features for action classification.

With the development of CNNs and RNNs, deep learning based methods significantly outperform the traditional methods. CNN-based methods [38], [18], [42], [39], [43], [44], [45] map a skeleton sequence into an image-like representation and use the network such as ResNet to extract the spatial and temporal features of the sequence for action recognition. RNN-based methods [46], [47], [48], [49], [50] take each frame as the input of a time step in recurrent neural networks to model the spatial and temporal correlations for action recognition.

Thanks to the development of graph convolutional networks to process structured data, GCN-based methods [4], [51], [5], [6], [52], [7], [8], [9], [10], [11], [12], [53] have been demonstrated to be effective for skeleton-based action recognition. The latest GCN-based methods can be divided into three categories. First, some methods design sophisticated GCN structures to better model the spatial and temporal features [10], [8], [53]. Liu *et al.* [10] leverage dense cross space-time edges as skip connections for unbiased long-range and unobstructed information propagation in spatial-temporal dimension. Zhang *et al.* [8] propose a context-aware GCN to consider a context term for each vertex by integrating information of all other vertices. Chen *et al.* [53] propose a channel-wise topology refinement graph convolution to learn different topologies and aggregate joint features in different channels. Second, some models aim at reducing computational cost for skeleton data [7], [9], [12]. Zhang *et al.* [7] explicitly introduce the high level semantics of joints into the network and build a strong and lightweight baseline for action recognition. Cheng *et al.* [9], [12] propose the lightweight graph operations to enhance the graph modeling ability. Cheng *et al.* [12] propose decoupling GCN to enhance the graph modeling ability without extra computation. Third, other works handle unsupervised learning [11], self-supervised learning [54] of skeleton based action recognition.

In this work, we attempt to integrate the interacted object into the skeleton-based action recognition framework to strengthen the human action recognition. A framework for joint training of interacted object localization and human action recognition is proposed, where the two tasks collaborate to promote each other.

C. Interacted Object Localization

In image-based scenarios, Gkioxari *et al.* [16] predict the interacted object location based on the appearance feature of a detected person with the supervision of volumes of interacted person-object box pairs. Li *et al.* [55] learn a binary score of interactiveness as a general knowledge for human object interaction detection. In [56], they hand-craft a rule to determine the interactiveness according to distance between humans and objects. In video-based scenarios, interacted object localization is barely explored due to the absence of interacted human-object bounding boxes. In this work, we study the interacted object localization for action recognition based on skeleton

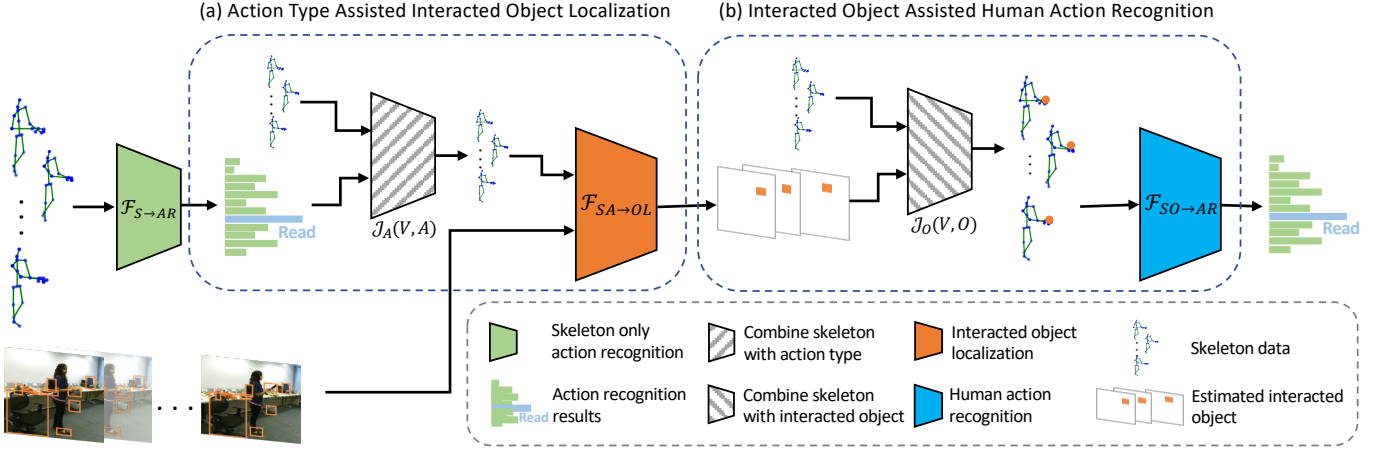


Fig. 2. Overview of our proposed joint task learning framework for robust human action recognition. Given a video sequence, we have its skeleton sequence and frame-level object detection results (obtained from an off-the-shelf object detector). A $\mathcal{F}_{S \rightarrow AR}$ model, *i.e.*, skeleton-only human action recognition model, generates a preliminary action classification score, followed by a joint learning procedure of (a) Action Type Assisted Interacted Object Localization and (b) Interacted Object Assisted Human Action Recognition. The two tasks are serialized together and collaborate to mutually promote each other.

data, without requiring ground-truth locations of the interacted object.

D. Joint Task Learning

Generic joint task learning is common and widely studied in computer vision. Many tasks have been studied such as the joint tasks of detection and classification [57], [58], depth estimation and image decomposition [59], segmentation and classification [60], and semantic segmentation and depth estimation from monocular images [61], [62], [63], [64]. In this paper, we propose a joint task learning framework for interacted object localization and human action recognition based on skeleton data.

III. PROPOSED JOINT LEARNING FRAMEWORK

In this section, we formulate the proposed joint learning framework for skeleton-based interacted object localization and human action recognition. Fig. 2 illustrates the proposed framework, where the *action type assisted interacted object localization* and the *interacted object assisted human action recognition* are serialized and collaborate to mutually promote each other. Given a video clip $X = \{x_t | t = 1, \dots, T\}$ with T frames, an object detector is applied on each frame to obtain the object candidates. The human skeleton data is captured by depth cameras. The object candidates are denoted by $O = \{o_{t,i} | t = 1, \dots, T, i = 1, \dots, N_o\}$ and the human skeletons are denoted by $V = \{v_{t,i} | t = 1, \dots, T, i = 1, \dots, N_v\}$, where N_o and N_v indicate the number of objects and human joints, respectively. If one frame contains more than one person, we split the frame to make sure each frame contains only one human skeleton as in [7]. Hereinafter, $S \rightarrow AR$ denotes skeleton-only human action recognition, $SA \rightarrow OL$ denotes integrating skeleton data and action type for interacted object localization, and $SO \rightarrow AR$ indicates integrating skeleton data and interacted object for human action recognition.

Previous skeleton-based methods [4], [5], [7], [8], [9], [10], [12] learn a classification model: $\tilde{A} = \mathcal{F}_{S \rightarrow AR}(V, \phi_{S \rightarrow AR})$

based only on skeleton data V , $\phi_{S \rightarrow AR}$ denotes the parameters and \tilde{A} is the estimated action recognition result. As mentioned before, we serialize the $SA \rightarrow OL$ and $SO \rightarrow AR$ tasks with the following formulation:

$$\tilde{A}^0 = \mathcal{F}_{S \rightarrow AR}^0(V, \phi_{S \rightarrow AR}^0), \quad (1)$$

$$\tilde{O}_{att}^1 = \mathcal{F}_{SA \rightarrow OL}^1(\mathcal{J}_A(V, \tilde{A}^0), \phi_{SA \rightarrow OL}^1), \quad (2)$$

$$\tilde{A}^2 = \mathcal{F}_{SO \rightarrow AR}^2(\mathcal{J}_O(V, \tilde{O}_{att}^1), \phi_{SO \rightarrow AR}^2). \quad (3)$$

In Eq. 1, model $\mathcal{F}_{S \rightarrow AR}^0$ generates the preliminary action classification result \tilde{A}^0 . In Eq. 2 of the next step, \mathcal{J}_A is a function of combining skeleton data V and action classification result \tilde{A}^0 , then $\mathcal{F}_{SA \rightarrow OL}^1$ takes the combined feature to boost the interacted object localization results \tilde{O}_{att}^1 . Then in Eq. 3, \mathcal{J}_O integrates the skeleton data V and the interacted object localization result \tilde{O}_{att}^1 from the previous step. The integrated feature is fed into $\mathcal{F}_{SO \rightarrow AR}^2$ for further human action recognition. ϕ denotes the parameters of these models.

We will introduce the $\mathcal{F}_{S \rightarrow AR}$ model in Sect. IV-B, which can be any skeleton-only action recognition model like ST-GCN [4], 2s-AGCN [5], or SGN [7]. The details of \mathcal{J}_A and $\mathcal{F}_{SA \rightarrow OL}$ will be presented in Sect. IV-C, and \mathcal{J}_O and $\mathcal{F}_{SO \rightarrow AR}$ will be presented in Sect. IV-D.

IV. TECHNICAL DETAILS

A. Data Preparation

Input: $\{X\} \mapsto$ **Output:** $\{O, V\}$

Given a video clip X with T frames, an object detector is applied on each frame to obtain the object candidates O . In this paper, we employ the Cascade RCNN [65] model trained on Object365 [66] to localize and detect objects. Object365 [66] is a newly proposed large-scale object detection dataset with 365 object classes, covering richer interactive objects than the COCO dataset [67]. For each frame, we select the first N_o (fixed) object candidates by detection scores. For more than N_o objects, we select those with higher object detection scores;

for less than N_o detected objects, we pad to N_o with the existing detected objects. The object features are composed of the bounding box, the confidence score, and the object category. In this paper, the RGB frames are only used for obtaining detected objects and the remaining modules are purely skeleton-based.

Following the previous works [7], the skeleton data V is captured by depth cameras and provided as 3D coordinates.

B. Skeleton-Only Action Recognition

Input: $\{V\} \mapsto$ **Output:** $\{\tilde{A}\}$

Previous effective skeleton-based action recognition models like ST-GCN [4], 2s-AGCN [5], or SGN [7] can be adopted. In this paper, we select SGN for its high computational efficiency. Next we recap the architecture of SGN.

SGN explicitly leverages the joint type and frame index as high-level semantics to enhance the feature representations. Given $V = \{v_{t,i} | t = 1, \dots, T, i = 1, \dots, N_v\}$ of T frames and N_v joints for each person, SGN obtains the dynamics representation $z_{t,i}$ of each joint:

$$z_{t,i} = \Phi_1(v_{t,i}) + \Phi_2(v_{t,i} - v_{t-1,i}), \quad (4)$$

where $v_{t,i} - v_{t-1,i}$ calculates the velocity of temporal neighboring joints, and Φ_1 and Φ_2 are two stacked fully connected (FC) layers to embed the position and velocity of joints to the same high dimensional space.

For the joint-level module, the joint dynamics feature j_m (i.e., one-hot vectors to indicate the index of the joint m) is concatenated with the semantics of joint type m at frame t as $z_{t,m} = z_{t,m} \oplus j_m$. Then, three adaptive GCN layers are stacked to exploit the correlations of different joints. In each GCN layer, the adjacency matrix S_t is calculated by the inner product of the transformed joint features as:

$$S_t(i, j) = \theta_z(z_{t,i})^T \cdot \phi_z(z_{t,j}), \quad (5)$$

where $\theta_z(\cdot)$ and $\phi_z(\cdot)$ are both implemented by a FC layer.

For the frame-level module, the frame index semantics (i.e., one-hot vectors to indicate the index of the frames) are incorporated into the joint representations $z_{t,i}$ to encode the order of the frames. Then the correlations across frames are modeled by two CNN layers. The first CNN layer is acting as a temporal convolution to model the dependencies of frames and the second layer maps the feature embedding to a high dimensional space. After the spatial-temporal feature embedding, a FC layer with Softmax acts as the action classification function.

C. Action Type Assisted Object Localization

Input: $\{(V, \tilde{A}), O\} \mapsto$ **Output:** $\{\tilde{O}_{att}\}$

We perform the interacted object localization task as a selection operation from the detected object candidates O based on the skeleton data V and the preliminary action classification result \tilde{A} in an unsupervised manner. The action type \tilde{A} can serve as the *state/attribute* of joints and enhance the representation ability over only 3D coordinates $\langle x, y, z \rangle$. For each joint of a frame, we incorporate the embedded feature

of the valuable action type cues together with the feature of the joints as:

$$f_{sa} = \mathcal{J}_A(v_{t,i}, \tilde{A}) = \Phi_j(v_{t,i}) \oplus \Phi_a(\tilde{A}), \quad (6)$$

where \tilde{A} denotes the action type vector, $v_{t,i}$ denotes the 3D coordinate of the i^{th} joint in the t^{th} frame of the skeleton sequence, Φ_j and Φ_a are constructed by two FCs to embed each joint and the action type to a 128-d feature vector, respectively, \oplus denotes the concatenation operation and f_{sa} denotes the combined 256-d feature.

The interacted object localization task is to select the most likely object from the candidates set O . We model the affinity between each joint and each object by calculating the inner-product of their embedded features, similar to Eq. 5. Therefore, for a person of N_v joints and N_o object candidates, we can obtain the affinity matrix $\mathcal{A} \in \mathbb{R}^{N_v \times N_o}$. Then, we perform max-pooling across the joints (rows) to obtain the affinity vector $o_{att} \in \mathbb{R}^{N_o}$, which denotes the affinity between the whole person and each object candidate. The Sigmoid operation is applied to normalize the affinity o_{att} to obtain the attention vector over objects as $\tilde{o}_{att} \in \mathbb{R}^{N_o}$. We denote the attention for all the T frames as $\tilde{O}_{att} \in \mathbb{R}^{T \times N_o}$.

Temporal Consistency Loss. We assume that given a video sequence of a person performing one action, the interacted object category is in general consistent over the time. Thus we propose a consistency loss across frames, which is defined as the variance of the categories of selected interacted object. Suppose the total number of object categories is N (For COCO-80 [67] dataset, $N=80$) and each video clip has T frames. We first obtain a matrix A of size $T \times N$ based on \tilde{O}_{att} , where $A(t, i)$ denotes the probability of being category i for frame t as the interacted object. Then, we first calculate the variance along the T dimension for each object category and then obtain the average value for the N object categories as the consistency loss.

D. Interacted Object Assisted Action Recognition

Input: $\{(V, \tilde{O}_{att}), O\} \mapsto$ **Output:** $\{\tilde{A}\}$

\tilde{O}_{att} serves as an attention to fuse the object candidates features. For each frame, we use the attention vector \tilde{o}_{att} as weights to fuse the features of the N_o candidate objects to obtain the feature representation of interacted object. Then we adopt a simple yet effective model \mathcal{J}_O , to integrate the re-weighted object information with the skeleton data for action classification. We extend the node feature from only the coordinate information to the combined representation of human joint coordinate and its interacted object. From the skeleton flow to skeleton+object flow, it carries more semantic information and stronger expression ability.

E. Loss Function

In our framework, $SA \rightarrow OL$ and $SO \rightarrow AR$ are serialized without sharing parameters across modules. For human action recognition, we obtain two outputs from $\mathcal{F}_{S \rightarrow AR}$ and $\mathcal{F}_{SO \rightarrow AR}$ modules. We average the two outputs as our ultimate action classification results. Our loss function is the summation

of the two action recognition losses \mathcal{L}_{a1} and \mathcal{L}_{a2} and the temporal consistency loss \mathcal{L}_{con} :

$$\mathcal{L} = \mathcal{L}_{a1} + \lambda_1 \mathcal{L}_{a2} + \lambda_2 \mathcal{L}_{con} \quad (7)$$

λ_1 and λ_2 are scalars to weight the losses, \mathcal{L}_{a1} and \mathcal{L}_{a2} are both cross-entropy losses of action classification.

V. EXPERIMENTS

A. Datasets

SYSU 3D Human-Object Interaction Dataset [17]. This dataset contains 480 video clips of 12 activities performed by 40 actors. For each video clip, the RGB frames, depth sequences and skeleton data are captured by a Kinect camera. We adopt the same evaluation protocols as in [17], *i.e.*, Cross Subject (CS) setting (half of the subjects for training and the rest for testing) and Same Subject (SS) setting (half of the samples of each subject for training and the rest for testing). For each setting, we report the mean accuracy results over 30 random splits as in [17].

NTU60 RGB+D Dataset [18]. NTU60 RGB+D is a large-scale and challenging human action dataset with 56,880 video clips together with the skeleton sequences of 60 actions performed by 40 subjects. The skeletons of each human is represented by 25 joints of 3D coordinates. In practice, we notice that NTU60 contains more than half non-interactive actions, such as “clap”, “salute” and “nod head/bow”, which is unfit for evaluating our model. Thus, we pick out 28 interactive actions to reorganize a new dataset with 26,368 video clips named **NTU60-HOI**. We have 17,789 video clips for training, 904 clips for validation, and 7,675 clips for testing.

We follow the previous experiment settings as [18], [7] to evaluate our model. For the Cross Subject (CS) setting, half of the 40 subjects are selected for training. For the Cross View (CV) setting, the skeleton sequences captured by two cameras are used for training, and those captured by the third camera are used for testing. Following [18], [7], we randomly select 10% for validation for both settings.

Northwestern-UCLA Dataset [19]. It contains 1,494 video clips covering 10 actions performed by 10 actors. The RGB, depth and skeleton data are captured by three Kinect cameras simultaneously. There are three views for each action and each person has 20 3D joints. We use the first two views for training and the third view for testing as in [19].

B. Implementation Details

Data Processing. For a fair comparison, we adopt the same strategy to process the skeleton sequence as in [7]. For each video clip, the skeleton data is translated to be invariant to the initial positions based on the first frame. During the training, we down-sample the video sequence by equally segment the entire sequence into k clips and randomly select one frame in each clip to generate a new sequence, and $k = 20, 20, 50, 50$ for NTU60 RGB+D, NTU60-HOI, SYSU-3D and NW-UCLA datasets, respectively. During testing, similar to [68], [7], we randomly generate 5 down-sampled sequences as the input and take the mean score as our ultimate action classification results. During training, data augmentation is performed by randomly

TABLE I
THE ABLATION STUDY RESULTS FOR $SA \rightarrow OL$ AND $SO \rightarrow AR$ MODULES ON THE SYSU-3D DATASET IN TERMS OF ACCURACY (%).

$SA \rightarrow OL$	$SO \rightarrow AR$	CS	SS
×	×	83.0	81.6
×	✓	86.5	84.4
✓	✓	88.5	87.5

rotating the skeleton data by some degrees for robustness as same as in [7].

For the object detection part, we directly adopt the trained model from the github repository¹ without fine-tuning. We also take the correlation between the action types and object categories as a dataset-specific prior to filter out objects that can hardly be interacted with. Take the NTU60 RGB+D dataset as an example, for each action type, we pick out the interactable object classes from all the object classes based on our prior knowledge. Finally, we get an union of the selected object classes for all the action types of this dataset. Then the object classes outside of the union set are filtered/discarded. We select $N_o = 10$ objects with detection scores greater than 0.1 for all the three datasets. For more than 10 objects, we select those with higher object detection scores; for less than 10 detected objects, we pad to 10 with the existing detected objects. We also add a *background* object category for those activities without interacted object.

Network Parameter Settings. For the $\mathcal{F}_{S \rightarrow AR}$ module, *i.e.*, the SGN model, we adopt the same network settings as in [7]. The number of neurons is set to 64 for Φ_1 and Φ_2 in Eq. 4 with not shared parameters. And the dimension of the semantics of joint type j_m is also 64. In Eq. 5 of joint-level, $\theta_z(\cdot)$ and $\phi_z(\cdot)$ transformed the joint features to a 256-d embedding space. The dimensions of the three stacked GCN layers are 128, 256 and 256, respectively. In the frame-level module, the dimension of the first CNN layer is 256 with kernel size of 3, and the second CNN layer is 512-d with kernel size of 1. The number of neurons of the frame index semantics is 256.

For the $\mathcal{F}_{SA \rightarrow OL}$ module, Φ_j and Φ_a in Eq. 6 have the dimension of 128. For the $\mathcal{F}_{SO \rightarrow AR}$ module, the dimension of the interacted object and the skeleton data are both of dimension of 256. We choose $\lambda_1 = 2$ and $\lambda_2 = 1$ for the loss function since $\mathcal{F}_{SO \rightarrow AR}$ could be harder to learn than $\mathcal{F}_{S \rightarrow AR}$.

Training Procedure. Our implementations are based on the Pytorch framework with one P100 GPU. We apply the Adam optimizer with the initial learning rate of 0.001 for all the datasets. Similar to [7], the learning rate decays by 1/10 at 60th, 90th and 110th epoch, respectively. The training epochs are set to 120, 120, 100, 100 and the batch sizes are set to 64, 64, 16, 16 for NTU60 RGB+D, NTU60-HOI, SYSU-3D and NW-UCLA, respectively. Following [7], we utilize label smoothing with a factor of 0.1 and cross entropy loss for action classification to train the networks.

¹<https://github.com/PaddlePaddle/PaddleDetection>

TABLE II

THE ABLATION STUDY RESULTS FOR THE TEMPORAL CONSISTENCY LOSS ON THE SYSU-3D DATASET IN TERMS OF ACCURACY (%).

Consistency Loss	CS	SS
×	86.4	85.8
✓	88.5	87.5

TABLE III

COMPARISONS OF THE ACCURACY (%) ON THE SYSU-3D DATASET WITH STATE-OF-THE-ART METHODS.

Methods	Year	CS	SS
VA-LSTM [43]	2017	77.5	76.9
ST-LSTM [69]	2018	76.5	-
GR-GCN [70]	2019	77.9	-
Two stream GCA-LSTM [71]	2017	77.9	-
SR-TSL [72]	2018	81.9	80.7
Baseline(SGN)	2020	83.0	81.6
Ours	-	88.5	87.5

C. Ablation Study

We evaluate the effectiveness of each component of our framework extensively on SYSU-3D dataset. The mean action classification accuracy results over 30 random splits on the Cross-Subject (CS) and Same-Subject (SS) setting of SYSU-3D dataset are reported. We choose SYSU-3D because this dataset is designed for studying human object interactions in videos and it is challenging with numerous background objects for interacted object localization. Note that, we only use joint data for training without any pretraining on other datasets.

1) *Effectiveness of joint learning*: To demonstrate the effectiveness of our joint task learning framework, we perform an ablation experiment on two main modules: $SA \rightarrow OL$ and $SO \rightarrow AR$ (in Tab. I). We have two main observations:

- 1) By integrating object information with skeleton data, *i.e.*, $SO \rightarrow AR$, the performance improves by 3.5% and 2.8% for the CS and SS settings, respectively.
- 2) By incorporating action type to assist interacted object localization, *i.e.*, $SA \rightarrow OL$, the performance improves by 2.0% and 3.1% for the CS and SS settings, respectively.

In summary, we can derive that interacted object localization and human action recognition can mutually promote each other in the joint learning framework.

2) *Effectiveness of temporal consistency loss*: We design two experiments (in Tab. II) to validate the effectiveness of temporal consistency loss introduced in Sect. IV-C. We have the observation that with consistency loss, the accuracy improves by 2.1% and 1.7% for the CS and SS settings, respectively. This verifies that employing the temporal consistency of interacted object categories is beneficial for localizing more accurate objects and in turn helps human action recognition.

D. Visualization of Interacted Object Localization

Due to the absence of ground-truth interacted human-object bounding boxes, we only provide the qualitative visualization results of the baseline model and our joint learning model in Fig. 3. The differences between these two models lie in the $SA \rightarrow OL$ module and the temporal consistency loss. We

TABLE IV

COMPARISONS OF THE ACCURACY (%) ON THE NTU60-HOI DATASET WITH STATE-OF-THE-ART METHODS. [†] DENOTES THE RESULT IS REPRODUCED BY US.

Methods	Year	CS	CV
2s-AGCN [†] [5]	2019	84.1	92.4
1s Shift-GCN [†] [9]	2020	84.5	92.8
MS-G3D Net [†] [10]	2020	85.7	92.9
Baseline(SGN) [†]	2020	85.3	92.4
Ours	-	87.7	94.8

TABLE V

COMPARISONS OF THE ACCURACY (%) ON THE FULL NTU60 RGB+D DATASET WITH STATE-OF-THE-ART METHODS.

Methods	Year	CS	CV
Lie Group [73]	2015	50.1	52.8
HBRNN-L [38]	2015	59.1	64.0
Part-Aware LSTM [18]	2016	62.9	70.3
ST-LSTM + Trust Gate [42]	2016	69.2	77.7
STA-LSTM [39]	2017	73.4	81.2
GCA-LSTM [74]	2017	74.4	82.8
Clips+CNN+MTLN [48]	2017	79.6	84.8
VA-LSTM [43]	2017	79.4	87.6
ElAtt-GRU [75]	2018	80.7	88.4
ST-GCN [4]	2018	81.5	88.3
DPRL+GCNN [76]	2018	83.5	89.8
SR-TSL [72]	2018	84.8	92.4
HCN [77]	2018	86.5	91.1
AGC-LSTM (joint) [78]	2019	87.5	93.5
AS-GCN [6]	2019	86.8	94.2
GR-GCN [70]	2019	87.5	94.3
2s-AGCN [5]	2019	88.5	95.1
VA-CNN [79]	2019	88.7	94.3
SGN [7]	2020	89.0	94.5
Advanced CA-GCN [8]	2020	83.5	91.4
1s Shift-GCN [9]	2020	87.8	95.1
2s Shift-GCN [9]	2020	89.7	96.0
4s Shift-GCN [9]	2020	90.7	96.5
MS-G3D Net [10]	2020	91.5	96.2
DC-GCN+ADG [12]	2020	90.8	96.6
CTR-GCN [53]	2021	92.4	96.8
STA-Hands [80]	2017	82.5	88.6
altered STA-Hands [81]	2018	84.8	90.6
Glimpse Cloud [68]	2018	86.6	93.2
PEM [51]	2018	91.7	95.2
SI-MM (RGB+Ske) [82]	2018	85.1	92.8
SI-MM (RGB+Ske+Flow) [82]	2018	92.6	97.9
Separable STA [83]	2019	92.2	94.6
P-I3D [84]	2020	93.0	95.4
Cross-Attention [85]	2020	84.2	89.3
VPN [86]	2020	95.5	98.0
Baseline (SGN [7])	2020	89.0	94.5
Ours	-	90.0	95.7

observe that the joint learning framework with temporal consistency loss provides more reasonable and robust interacted object localization results over the baseline method.

The action type of the four rows in Fig. 3 are “moving chair”, “mopping”, “sweeping” and “taking from wallet”. The upper three rows show that our joint learning framework obtains more consistent results, while the baseline model may change the interacted object along with the person movement. We also visualize the cases in the last row that the wallet is undetected, both the baseline method and ours fail. It inspires us to exploit a more general and robust interacted object detector in videos in future works.

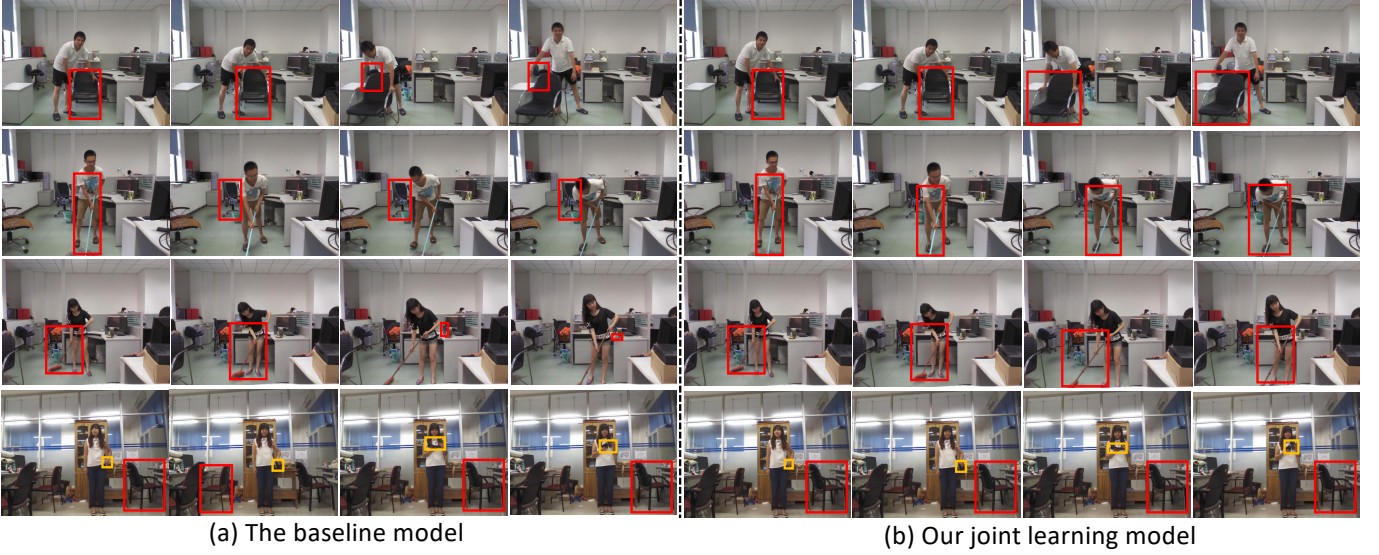


Fig. 3. Visualization results of the interacted object localization. The left rows are from the baseline model and the right rows are from ours. The red boxes indicate the estimated interacted object, the yellow boxes on the last row indicate the undetected interacted object.

TABLE VI
COMPARISONS OF THE ACCURACY (%) ON THE NW-UCLA DATASET
WITH STATE-OF-THE-ART METHODS.

Methods	Year	Accuracy
Lie Group [73]	2014	74.2
Actionlet ensemble [87]	2014	76.0
Visualization CNN [49]	2017	86.1
Ensemble TS-LSTM [88]	2017	89.2
2s AGC-LSTM [78]	2019	93.3
4s Shift-GCN [9]	2020	94.6
DC-GCN+ADG [12]	2020	95.3
CTR-GCN [53]	2021	96.5
NKTM [89]	2015	85.6
HPM+TM [90]	2016	91.0
Glimpse Cloud [68]	2018	90.1
Separable STA [83]	2019	92.4
P-I3D [84]	2019	93.1
VPN [86]	2020	93.5
Baseline(SGN)-joint	2020	92.5
Ours-joint	-	95.7
Ours-bone	-	94.6
Ours-2stream	-	97.2

E. Comparisons with the State-of-the-arts

We compare our joint learning framework with other state-of-the-art models on SYSU-3D, NTU60-HOI, full NTU60 RGB+D and NW-UCLA datasets in Tab. III, Tab. IV, Tab. V and Tab. VI, respectively.

1) *SYSU-3D*: SYSU-3D is focusing on human-object interactions in videos. As shown in Tab. III, we only utilize the joint feature without any pretraining on NTU-60 dataset for a fair comparison with the baseline model SGN [7]. Our proposed joint learning framework outperforms the baseline method by 5.5% and 5.9% for the CS and SS settings and sets up a new state-of-the-art.

2) *NTU60-HOI*: NTU60 RGB+D is a large scale human activity dataset and we construct a subset dataset NTU60-HOI with only the interactive actions. We treat SGN [7] as a strong

baseline and show the comparison in Tab. IV. Our framework outperforms the baseline by 2.4% and 2.4% for the CS and CV settings, respectively. We also re-produce the results of some other latest approaches [5], [9], [10] using their provided source code. We can see that our method achieves the state-of-the-art performance. It confirms the effectiveness of our method on large-scale video action benchmarks.

3) *NTU60 RGB+D*: For the full NTU60 RGB+D dataset, we present the comparisons in Tab. V. The methods in the **upper rows** belong to the skeleton-only based methods. Particularly, the 4s Shift-GCN [9], DC-GCN+ADG [12] and CTR-GCN [53] models ensemble the results of 4 streams: joint, bone, joint motion and bone motion while we only use the joint stream as in [7]. MS-G3D Net [10] leverages dense cross space-time information propagation with high computational complexity. In the **middle rows**, we present those methods using RGB information or multi-modality features. Particularly, PEM [51] takes the estimated pose heatmap from RGB frames as input for action prediction. SI-MM (RGB+Ske) [82] fuses the RGB information and the skeleton in multiple streams and SI-MM (RGB+Ske+Flow) uses extra optical flow data. Separable STA [83], P-I3D [84], Cross-Attention [85], and VPN [86] all design sophisticated visual backbone networks (*i.e.*, I3D [24]) pre-trained on the very large-scale dataset Kinetics-400 [31]. The **bottom two rows** show the performance of the baseline and our proposed method. Our method outperforms the baseline method by 1.0% and 1.2% for the CS and CV settings, respectively.

4) *Northwestern-UCLA*: For the NW-UCLA dataset, we choose the SGN [7] as our baseline and implement our joint learning framework based on it. In Tab. VI, the methods in the **upper rows** only use skeleton data. The methods in the **middle rows** utilize RGB information or multi-modality information. Particularly, separable STA [83], P-I3D [84], and VPN [86] all design sophisticated visual backbone networks pre-trained on

the very large-scale dataset Kinetics-400 [31]. In the **bottom rows**, “joint” means only utilizing skeleton joints data, “bone” means only utilizing the bones (physical connections between joints) feature as introduced in [5] and “2stream” means the fusion of joint-stream and bone-stream as in [5]. Note that, DC-GCN+ADG [12] ensembles 4 streams of joint, bone, joint motion and bone motion as in [52]. Since [7] implicitly calculates the velocity of joints similar to the joint/bone motion design, we only report the fusion result of joint-stream and bone-stream for a fair comparison. Our framework brings gains of 3.2% for the joint stream, 4.7% for the fusion stream over the baseline model and sets up a new state-of-the-art.

VI. LIMITATIONS AND FUTURE WORKS

In this work, we verify the effectiveness of the joint learning framework for interacted object localization and human action recognition using skeleton data. We discuss some limitations and future works here.

- Our implementation for interacted object localization is based on the preliminary object detection results. The failure of object detection will hurt the subsequent interacted object localization. Thus a more general and robust interacted object detector in videos is desired.
- Our framework can be extended to other modalities, such as RGB/RGB+D video sequences. The motion information between frames can be better exploited for localizing interacted object.
- By integrating interacted object with the skeleton data, we extend the pose flow to the pose+object flow. The *semantics* of human joints interacting with the objects could be better explored.

VII. CONCLUSION

In this work, we propose a joint learning framework for “interacted object localization” and “human action recognition” based on skeleton data without ground-truth of interacted object. The two tasks are serialized and collaborate to promote each other in an end-to-end manner. To make up for the absence of labels of interacted human-object boxes, we introduce the temporal consistency loss to strengthen the interacted object localization. Quantitative and qualitative results show that our joint learning framework outperforms the baseline models for action recognition by a large margin and also achieves reasonable interacted object localization results. We hope that our work will inspire more future works on interacted object localization and human action recognition.

REFERENCES

- [1] R. Poppe, “A survey on vision-based human action recognition,” *Image and vision computing*, vol. 28, no. 6, pp. 976–990, 2010.
- [2] D. Weinland, R. Ronfard, and E. Boyer, “A survey of vision-based methods for action representation, segmentation and recognition,” *Computer vision and image understanding*, vol. 115, no. 2, pp. 224–241, 2011.
- [3] J. K. Aggarwal and M. S. Ryoo, “Human activity analysis: A review,” *ACM Computing Surveys (CSUR)*, vol. 43, no. 3, pp. 1–43, 2011.
- [4] S. Yan, Y. Xiong, and D. Lin, “Spatial temporal graph convolutional networks for skeleton-based action recognition,” *arXiv preprint arXiv:1801.07455*, 2018.
- [5] L. Shi, Y. Zhang, J. Cheng, and H. Lu, “Two-stream adaptive graph convolutional networks for skeleton-based action recognition,” in *CVPR*, 2019, pp. 12 026–12 035.
- [6] M. Li, S. Chen, X. Chen, Y. Zhang, Y. Wang, and Q. Tian, “Actional-structural graph convolutional networks for skeleton-based action recognition,” in *CVPR*, 2019, pp. 3595–3603.
- [7] P. Zhang, C. Lan, W. Zeng, J. Xing, J. Xue, and N. Zheng, “Semantics-guided neural networks for efficient skeleton-based human action recognition,” in *CVPR*, 2020, pp. 1112–1121.
- [8] X. Zhang, C. Xu, and D. Tao, “Context aware graph convolution for skeleton-based action recognition,” in *CVPR*, 2020, pp. 14 333–14 342.
- [9] K. Cheng, Y. Zhang, X. He, W. Chen, J. Cheng, and H. Lu, “Skeleton-based action recognition with shift graph convolutional network,” in *CVPR*, 2020, pp. 183–192.
- [10] Z. Liu, H. Zhang, Z. Chen, Z. Wang, and W. Ouyang, “Disentangling and unifying graph convolutions for skeleton-based action recognition,” in *CVPR*, 2020, pp. 143–152.
- [11] K. Su, X. Liu, and E. Shlizerman, “Predict & cluster: Unsupervised skeleton based action recognition,” in *CVPR*, 2020, pp. 9631–9640.
- [12] K. Cheng, Y. Zhang, C. Cao, L. Shi, J. Cheng, and H. Lu, “Decoupling gcw with dropgraph module for skeleton-based action recognition,” in *ECCV*, 2020.
- [13] J. Materzynska, T. Xiao, R. Herzig, H. Xu, X. Wang, and T. Darrell, “Something-else: Compositional action recognition with spatial-temporal interaction networks,” in *CVPR*, 2020, pp. 1049–1059.
- [14] J. Tang, J. Xia, X. Mu, B. Pang, and C. Lu, “Asynchronous interaction aggregation for action detection,” *arXiv preprint arXiv:2004.07485*, 2020.
- [15] Y.-L. Li, L. Xu, X. Liu, X. Huang, Y. Xu, S. Wang, H.-S. Fang, Z. Ma, M. Chen, and C. Lu, “Pastanet: Toward human activity knowledge engine,” in *CVPR*, 2020, pp. 382–391.
- [16] G. Gkioxari, R. Girshick, P. Dollár, and K. He, “Detecting and recognizing human-object interactions,” in *CVPR*, 2018, pp. 8359–8367.
- [17] J.-F. Hu, W.-S. Zheng, J. Lai, and J. Zhang, “Jointly learning heterogeneous features for rgb-d activity recognition,” in *CVPR*, 2015, pp. 5344–5352.
- [18] A. Shahroudy, J. Liu, T.-T. Ng, and G. Wang, “Ntu rgb+ d: A large scale dataset for 3d human activity analysis,” in *CVPR*, 2016, pp. 1010–1019.
- [19] J. Wang, X. Nie, Y. Xia, Y. Wu, and S.-C. Zhu, “Cross-view action modeling, learning and recognition,” in *CVPR*, 2014, pp. 2649–2656.
- [20] S. Ji, W. Xu, M. Yang, and K. Yu, “3d convolutional neural networks for human action recognition,” *TPAMI*, vol. 35, no. 1, pp. 221–231, 2012.
- [21] D. Tran, L. D. Bourdev, R. Fergus, L. Torresani, and M. Paluri, “C3d: generic features for video analysis,” *CoRR, abs/1412.0767*, vol. 2, no. 7, p. 8, 2014.
- [22] G. W. Taylor, R. Fergus, Y. LeCun, and C. Bregler, “Convolutional learning of spatio-temporal features,” in *ECCV*. Springer, 2010, pp. 140–153.
- [23] G. Varol, I. Laptev, and C. Schmid, “Long-term temporal convolutions for action recognition,” *TPAMI*, vol. 40, no. 6, pp. 1510–1517, 2017.
- [24] J. Carreira and A. Zisserman, “Quo vadis, action recognition? a new model and the kinetics dataset,” in *CVPR*, 2017, pp. 6299–6308.
- [25] Z. Qiu, T. Yao, and T. Mei, “Learning spatio-temporal representation with pseudo-3d residual networks,” in *ICCV*, 2017, pp. 5533–5541.
- [26] A. Diba, M. Fayyaz, V. Sharma, M. Mahdi Arzani, R. Yousefzadeh, J. Gall, and L. Van Gool, “Spatio-temporal channel correlation networks for action classification,” in *ECCV*, 2018, pp. 284–299.
- [27] D. Tran, H. Wang, L. Torresani, J. Ray, Y. LeCun, and M. Paluri, “A closer look at spatiotemporal convolutions for action recognition,” in *CVPR*, 2018, pp. 6450–6459.
- [28] S. Xie, C. Sun, J. Huang, Z. Tu, and K. Murphy, “Rethinking spatiotemporal feature learning for video understanding,” *arXiv preprint arXiv:1712.04851*, vol. 1, no. 2, p. 5, 2017.
- [29] R. Christoph and F. A. Pinz, “Spatiotemporal residual networks for video action recognition,” *Neurips*, pp. 3468–3476, 2016.
- [30] K. Soomro, A. R. Zamir, and M. Shah, “Ucf101: A dataset of 101 human actions classes from videos in the wild,” *arXiv preprint arXiv:1212.0402*, 2012.
- [31] W. Kay, J. Carreira, K. Simonyan, B. Zhang, C. Hillier, S. Vijayanarasimhan, F. Viola, T. Green, T. Back, P. Natsev *et al.*, “The kinetics human action video dataset,” *arXiv preprint arXiv:1705.06950*, 2017.
- [32] C. Gu, C. Sun, D. A. Ross, C. Vondrick, C. Pantofaru, Y. Li, S. Vijayanarasimhan, G. Toderici, S. Ricco, R. Sukthankar *et al.*, “Ava: A video dataset of spatio-temporally localized atomic visual actions,” in *CVPR*, 2018, pp. 6047–6056.

- [33] B. G. Fabian Caba Heilbron, Victor Escorcia and J. C. Niebles, "ActivityNet: A large-scale video benchmark for human activity understanding," in *CVPR*, 2015, pp. 961–970.
- [34] P. Gupta, A. Thatipelli, A. Aggarwal, S. Maheshwari, N. Trivedi, S. Das, and R. K. Sarvadevabhatla, "Quo vadis, skeleton action recognition?" 2020.
- [35] C. Feichtenhofer, H. Fan, J. Malik, and K. He, "Slowfast networks for video recognition," in *CVPR*, 2019, pp. 6202–6211.
- [36] R. Hou, C. Chen, and M. Shah, "Tube convolutional neural network (t-cnn) for action detection in videos," in *ICCV*, 2017, pp. 5822–5831.
- [37] R. Vemulapalli, F. Arrate, and R. Chellappa, "Human action recognition by representing 3d skeletons as points in a lie group," in *CVPR*, 2014, pp. 588–595.
- [38] Y. Du, W. Wang, and L. Wang, "Hierarchical recurrent neural network for skeleton based action recognition," in *CVPR*, 2015, pp. 1110–1118.
- [39] S. Song, C. Lan, J. Xing, W. Zeng, and J. Liu, "An end-to-end spatio-temporal attention model for human action recognition from skeleton data," *arXiv preprint arXiv:1611.06067*, 2016.
- [40] J. Wang, Z. Liu, Y. Wu, and J. Yuan, "Mining actionlet ensemble for action recognition with depth cameras," in *CVPR*. IEEE, 2012, pp. 1290–1297.
- [41] C. Xie, C. Li, B. Zhang, C. Chen, J. Han, C. Zou, and J. Liu, "Memory attention networks for skeleton-based action recognition," *arXiv preprint arXiv:1804.08254*, 2018.
- [42] J. Liu, A. Shahroudy, D. Xu, and G. Wang, "Spatio-temporal lstm with trust gates for 3d human action recognition," in *ECCV*. Springer, 2016, pp. 816–833.
- [43] P. Zhang, C. Lan, J. Xing, W. Zeng, J. Xue, and N. Zheng, "View adaptive recurrent neural networks for high performance human action recognition from skeleton data," in *ICCV*, 2017, pp. 2117–2126.
- [44] S. Li, W. Li, C. Cook, C. Zhu, and Y. Gao, "Independently recurrent neural network (indrn): Building a longer and deeper rnn," in *CVPR*, 2018, pp. 5457–5466.
- [45] C. Cao, C. Lan, Y. Zhang, W. Zeng, H. Lu, and Y. Zhang, "Skeleton-based action recognition with gated convolutional neural networks," *TCSVT*, vol. 29, no. 11, pp. 3247–3257, 2018.
- [46] H. Liu, J. Tu, and M. Liu, "Two-stream 3d convolutional neural network for skeleton-based action recognition," *arXiv preprint arXiv:1705.08106*, 2017.
- [47] T. S. Kim and A. Reiter, "Interpretable 3d human action analysis with temporal convolutional networks," in *CVPRW*. IEEE, 2017, pp. 1623–1631.
- [48] Q. Ke, M. Bennamoun, S. An, F. Sohel, and F. Boussaid, "A new representation of skeleton sequences for 3d action recognition," in *CVPR*, 2017, pp. 3288–3297.
- [49] M. Liu, H. Liu, and C. Chen, "Enhanced skeleton visualization for view invariant human action recognition," *Pattern Recognition*, vol. 68, pp. 346–362, 2017.
- [50] C. Li, Q. Zhong, D. Xie, and S. Pu, "Skeleton-based action recognition with convolutional neural networks," in *ICMEW*. IEEE, 2017, pp. 597–600.
- [51] M. Liu and J. Yuan, "Recognizing human actions as the evolution of pose estimation maps," in *CVPR*, 2018, pp. 1159–1168.
- [52] L. Shi, Y. Zhang, J. Cheng, and H. Lu, "Skeleton-based action recognition with directed graph neural networks," in *CVPR*, 2019, pp. 7912–7921.
- [53] Y. Chen, Z. Zhang, C. Yuan, B. Li, Y. Deng, and W. Hu, "Channel-wise topology refinement graph convolution for skeleton-based action recognition," in *Proceedings of the IEEE/CVF International Conference on Computer Vision*, 2021, pp. 13 359–13 368.
- [54] L. Lin, S. Song, W. Yang, and J. Liu, "Ms2l," *ACM Multimedia*, Oct 2020. [Online]. Available: <http://dx.doi.org/10.1145/3394171.3413548>
- [55] Y.-L. Li, S. Zhou, X. Huang, L. Xu, Z. Ma, H.-S. Fang, Y. Wang, and C. Lu, "Transferable interactiveness knowledge for human-object interaction detection," in *CVPR*, 2019, pp. 3585–3594.
- [56] Y. Hu, S. Chen, X. Chen, Y. Zhang, and X. Gu, "Neural message passing for visual relationship detection," in *ICMLW*, 2019.
- [57] R. Girshick, "Fast r-cnn," in *ICCV*, 2015, pp. 1440–1448.
- [58] K. He, G. Gkioxari, P. Dollár, and R. Girshick, "Mask r-cnn," in *ICCV*, 2017, pp. 2961–2969.
- [59] S. Kim, K. Park, K. Sohn, and S. Lin, "Unified depth prediction and intrinsic image decomposition from a single image via joint convolutional neural fields," in *ECCV*. Springer, 2016, pp. 143–159.
- [60] I. Misra, A. Shrivastava, A. Gupta, and M. Hebert, "Cross-stitch networks for multi-task learning," in *CVPR*, 2016, pp. 3994–4003.
- [61] L. Ladicky, J. Shi, and M. Pollefeys, "Pulling things out of perspective," in *CVPR*, 2014, pp. 89–96.
- [62] P. Wang, X. Shen, Z. Lin, S. Cohen, B. Price, and A. L. Yuille, "Towards unified depth and semantic prediction from a single image," in *CVPR*, 2015, pp. 2800–2809.
- [63] A. Kendall, Y. Gal, and R. Cipolla, "Multi-task learning using uncertainty to weigh losses for scene geometry and semantics," in *CVPR*, 2018, pp. 7482–7491.
- [64] Z. Zhang, Z. Cui, C. Xu, Z. Jie, X. Li, and J. Yang, "Joint task-recursive learning for semantic segmentation and depth estimation," in *ECCV*, 2018, pp. 235–251.
- [65] Z. Cai and N. Vasconcelos, "Cascade r-cnn: Delving into high quality object detection," in *CVPR*, 2018, pp. 6154–6162.
- [66] S. Shao, Z. Li, T. Zhang, C. Peng, G. Yu, X. Zhang, J. Li, and J. Sun, "Objects365: A large-scale, high-quality dataset for object detection," in *ICCV*, 2019, pp. 8430–8439.
- [67] T.-Y. Lin, M. Maire, S. Belongie, J. Hays, P. Perona, D. Ramanan, P. Dollár, and C. L. Zitnick, "Microsoft coco: Common objects in context," in *ECCV*. Springer, 2014, pp. 740–755.
- [68] F. Baradel, C. Wolf, J. Mille, and G. W. Taylor, "Glimpse clouds: Human action recognition from unstructured feature points," in *CVPR*, 2018, pp. 469–478.
- [69] J. Liu, A. Shahroudy, D. Xu, A. C. Kot, and G. Wang, "Skeleton-based action recognition using spatio-temporal lstm network with trust gates," *TPAMI*, vol. 40, no. 12, pp. 3007–3021, 2017.
- [70] X. Gao, W. Hu, J. Tang, J. Liu, and Z. Guo, "Optimized skeleton-based action recognition via sparsified graph regression," in *ACM Multimedia*, 2019, pp. 601–610.
- [71] J. Liu, G. Wang, L.-Y. Duan, K. Abdiyeva, and A. C. Kot, "Skeleton-based human action recognition with global context-aware attention lstm networks," *TIP*, vol. 27, no. 4, pp. 1586–1599, 2017.
- [72] C. Si, Y. Jing, W. Wang, L. Wang, and T. Tan, "Skeleton-based action recognition with spatial reasoning and temporal stack learning," in *ECCV*, 2018, pp. 103–118.
- [73] V. Veeriah, N. Zhuang, and G.-J. Qi, "Differential recurrent neural networks for action recognition," in *CVPR*, 2015, pp. 4041–4049.
- [74] J. Liu, G. Wang, P. Hu, L.-Y. Duan, and A. C. Kot, "Global context-aware attention lstm networks for 3d action recognition," in *CVPR*, 2017, pp. 1647–1656.
- [75] P. Zhang, J. Xue, C. Lan, W. Zeng, Z. Gao, and N. Zheng, "Adding attentiveness to the neurons in recurrent neural networks," in *ECCV*, 2018, pp. 135–151.
- [76] Y. Tang, Y. Tian, J. Lu, P. Li, and J. Zhou, "Deep progressive reinforcement learning for skeleton-based action recognition," in *CVPR*, 2018, pp. 5323–5332.
- [77] C. Li, Q. Zhong, D. Xie, and S. Pu, "Co-occurrence feature learning from skeleton data for action recognition and detection with hierarchical aggregation," *arXiv preprint arXiv:1804.06055*, 2018.
- [78] C. Si, W. Chen, W. Wang, L. Wang, and T. Tan, "An attention enhanced graph convolutional lstm network for skeleton-based action recognition," in *CVPR*, 2019, pp. 1227–1236.
- [79] P. Zhang, C. Lan, J. Xing, W. Zeng, J. Xue, and N. Zheng, "View adaptive neural networks for high performance skeleton-based human action recognition," *TPAMI*, vol. 41, no. 8, pp. 1963–1978, 2019.
- [80] Baradel, Fabien and Wolf, Christian and Mille, Julien, "Human action recognition: Pose-based attention draws focus to hands," in *ICCVW*, 2017, pp. 604–613.
- [81] F. Baradel, C. Wolf, and J. Mille, "Human activity recognition with pose-driven attention to rgb," in *BMVC*, 2018.
- [82] S. Song, C. Lan, J. Xing, W. Zeng, and J. Liu, "Skeleton-indexed deep multi-modal feature learning for high performance human action recognition," in *ICME*. IEEE, 2018, pp. 1–6.
- [83] S. Das, R. Dai, M. Koperski, L. Minciullo, L. Garattoni, F. Bremond, and G. Francesca, "Toyota smarhome: Real-world activities of daily living," in *ICCV*, 2019, pp. 833–842.
- [84] S. Das, A. Chaudhary, F. Bremond, and M. Thonnat, "Where to focus on for human action recognition?" in *WACV*, 2019, pp. 71–80.
- [85] Y. Fan, S. Weng, Y. Zhang, B. Shi, and Y. Zhang, "Context-aware cross-attention for skeleton-based human action recognition," *IEEE Access*, vol. 8, pp. 15 280–15 290, 2020.
- [86] S. Das, S. Sharma, R. Dai, F. Bremond, and M. Thonnat, "Vpn: Learning video-pose embedding for activities of daily living," in *ECCV*. Springer, 2020, pp. 72–90.
- [87] J. Wang, Z. Liu, Y. Wu, and J. Yuan, "Learning actionlet ensemble for 3d human action recognition," *TPAMI*, vol. 36, no. 5, pp. 914–927, 2013.
- [88] I. Lee, D. Kim, S. Kang, and S. Lee, "Ensemble deep learning for skeleton-based action recognition using temporal sliding lstm networks," in *ICCV*, 2017, pp. 1012–1020.

- [89] H. Rahmani and A. Mian, “Learning a non-linear knowledge transfer model for cross-view action recognition,” in *CVPR*, 2015, pp. 2458–2466.
- [90] Rahmani, Hossein and Mian, Ajmal, “3d action recognition from novel viewpoints,” in *CVPR*, 2016, pp. 1506–1515.